

# New Insights into the Role of Inflammatory Pathways and Immune Cell Infiltration in Sleep Deprivation-Induced Atrial Fibrillation: An Integrated Bioinformatics and Experimental Study

Junqing Liang <sup>1,2</sup>, Baopeng Tang <sup>1,2</sup>, Jun Shen <sup>1,2</sup>, Manzeremu Rejiepu<sup>1,2</sup>, Yankai Guo <sup>1,2</sup>, Xiaoyan Wang<sup>1,2</sup>, Shijie Shao<sup>1,2</sup>, Fei Guo<sup>3</sup>, Qin Wang<sup>4</sup>, Ling Zhang <sup>1</sup>

<sup>1</sup>Xinjiang Key Laboratory of Cardiac Electrophysiology and Cardiac Remodeling, The First Affiliated Hospital of Xinjiang Medical University, Urumqi, Xinjiang, People's Republic of China; <sup>2</sup>Cardiac Pacing and Electrophysiology Department, The First Affiliated Hospital of Xinjiang Medical University, Urumqi, Xinjiang, People's Republic of China; <sup>3</sup>Department of Cardiology, The First Affiliated Hospital of USTC, Division of Life Sciences and Medicine, University of Science and Technology of China, Hefei, People's Republic of China; <sup>4</sup>Department of Geriatrics and Cadre Ward, Second Affiliated Hospital of Xinjiang Medical University, Urumqi, Xinjiang, People's Republic of China

Correspondence: Qin Wang; Ling Zhang, Email w2036661q@126.com; ydzhangling@126.com

**Background:** The common occurrence of atrial fibrillation (AF) as a cardiac arrhythmia, along with its link to sleep deprivation (SD), is gaining more acknowledgment. Even with progress in comprehending the development of AF, the molecular connections between SD and AF are still not well-defined. The objective of this research was to pinpoint the shared molecular routes responsible for SD-induced AF and investigate possible treatment targets.

**Methods:** Utilizing bioinformatics, we examined two transcriptome datasets from the Gene Expression Omnibus (GEO) database to pinpoint genes with differential expression (DEGs) common to SD and AF. Analyses focusing on functional enrichment, such as Gene Ontology (GO) and Kyoto Encyclopedia of Genes and Genomes (KEGG), were conducted to pinpoint crucial biological mechanisms and pathways. Furthermore, we utilized immunofluorescence and Western blot techniques to evaluate YBX1 expression and its role in activating NLRP3 inflammasomes in a rat model induced by SD.

**Results:** A total of 540 common DEGs were precisely identified between the AF and SD data collections. Studies emphasizing functional enrichment have highlighted the significance of inflammation pathways, particularly the NOD-like receptor signaling route. The application of machine learning uncovered four crucial genes—CDC5L, MAPK14, RAB5A, and YBX1—with YBX1 becoming the predominant gene in diagnostic processes. Investigating immune penetration revealed significant connections between YBX1 expression and specific immune cell types, notably CD8+ T cells and M1 macrophages. Live studies have demonstrated that SD amplifies the atrial electrical rearrangement, structural changes, the infiltration of inflammatory cells, and the heightened presence of YBX1 along with inflammasome elements.

**Conclusion:** The research pinpoints YBX1 as a crucial gene in SD-related AF, possibly influencing its impact via the NOD-like receptor signaling route and the invasion of immune cells. The results offer crucial understanding of the molecular processes behind AF and propose YBX1 as a possible treatment focus to reduce the risk of AF caused by SD.

**Keywords:** atrial fibrillation, sleep deprivation, bioinformatic analysis, inflammation, YBX1

## Introduction

Atrial Fibrillation (AF) stands as the predominant form of persistent heart rhythm disorders, characterized by rapid and erratic electrical impulses in the atria, resulting in diminished effectiveness of atrial contractions. Such disturbances in cardiac rhythms notably reduce a patient's life quality and substantially increase their likelihood of severe issues, including stroke, heart failure, and general mortality.<sup>1</sup> Despite major progress in AF management via enhanced diagnostic techniques and treatment methods, the fundamental biological processes causing this arrhythmia remain largely elusive.

AF originates from a myriad of causes, its development and advancement being influenced by a multifaceted combination of lifestyle, environmental factors, inflammation, and metabolic concerns.<sup>2,3</sup> Consequently, further investigation into the molecular mechanisms involved in AF, particularly gene expression, is vital for devising innovative and successful treatment strategies.

The prevalence of Sleep deprivation (SD) as a health concern grows in contemporary society, increasingly associated by research with the beginning and worsening of diverse cardiovascular ailments.<sup>4,5</sup> Latest research indicates that diminished sleep quality typically extends AF episodes beyond the following day. With deteriorating slumber, the duration of AF episodes also declines.<sup>6</sup> While the complete processes remain unclear, they are presumed to encompass various routes, encompassing the stimulation of the sympathetic nervous system, enhancement of inflammation, and intensification of oxidative stress.<sup>7-9</sup> Together, these elements lead to increased vulnerability to AF among those who have had extended durations of insufficient sleep.

Previous studies have shown that inflammation markedly affects both SD and AF. In a mouse model for SD, SD initiates a concentration of neutrophils, leading to a significant rise in pro-inflammatory cytokines Interleukin-6 and IL-17, triggering a broad inflammatory response.<sup>10</sup> Additionally, in patients with AF, there was a significant rise in inflammatory components such as CRP, IL-6, IL-8, and TNF, all of which have a direct impact on cardiomyocytes, leading to alterations in atrial architecture and electrical operations.<sup>11</sup> Importantly, the emergence of inflammation triggers AF and also assists in the reorganization of the atrium by amplifying the inflammatory response, leading to a continuous cycle termed the “atrial fibrillation triggers atrial fibrillation” phenomenon.<sup>11</sup> Given the substantial effect of inflammation on SD and AF, it seems reasonable to propose that SD might elevate the risk of AF by initiating the inflammatory response.

High-throughput sequencing technologies have transformed research into intricate diseases, facilitating an in-depth exploration of the molecular foundations of conditions like AF and SD.<sup>12</sup> Specifically, the use of bioinformatics analysis is now crucial in integrating diverse genomic data to pinpoint essential genes and signaling routes in disease development.<sup>13</sup> In our study, we methodically investigated the inflammatory response mechanism between SD and AF using bioinformatics techniques derived from gene expression records in the Gene Expression Omnibus (GEO) database. This research focuses on examining prospective biomarkers and pinpointing potential treatment targets, laying a theoretical groundwork for understanding molecular processes and clinical treatment approaches for associated illnesses.

## Materials and Methods

### Data Collection

The GEO database (<https://www.ncbi.nlm.nih.gov/geo/>) yielded four distinct transcriptome datasets: GSE79768, GSE98582, GSE41177, and GSE56931. GSE79768 and GSE98582 were utilized for training, whereas GSE41177 and GSE56931 functioned for independent verification. In the process of evaluating the dataset within the GEO database, our approach was as follows: initially, we designated the search phrases “atrial fibrillation” or “sleep deprivation” to verify the dataset’s pertinence to the research subject. Secondly, to enhance the dataset’s relevance and precision, we confined the species to human subjects. Furthermore, our focus was solely on microarray or RNA sequence datasets, given their critical significance in gene expression research. Ultimately, it was guaranteed that the chosen datasets possessed ample sample sizes and distinct control groups to fulfill statistical analysis requirements and enhance the dependability of the study findings. Comprehensive data from the dataset are presented in [Table 1](#).

**Table 1** A Summary of Microarray Information

GEO Number	Platform	Control Samples	Disease Samples
GSE79768	GPL570	12	14
GSE98582	GPL6244	213	342
GSE41177	GPL570	6	32
GSE56931	GPL10379	129	120

## Acquisition of Microarray Data and Identification of DEGs

“GEOquery” (version 2.72.0) was employed to systematically gather and analyze microarray datasets. Genes exhibiting differential expression (DEGs) were pinpointed using the “limma” software (version 3.60.4).<sup>14</sup> Visualization of DEGs, including volcano plots and heatmaps, was performed using the “ggplot2” package (version 3.5.1).<sup>15</sup> Utilizing the online resource Xiantaozi (<https://www.xiantaozi.com/>), a Venn diagram was developed to pinpoint and examine the common DEGs in sleep deprivation (SD) and atrial fibrillation (AF), uncovering possible molecular links between these two states.

## Analysis of Functional Enrichment

To elucidate the roles of identified targets, functional enrichment analyses were conducted using Gene Ontology (GO) and Kyoto Encyclopedia of Genes and Genomes (KEGG) pathway analysis.<sup>16–18</sup> The GO analysis encompassed areas such as molecular functions (MF), biological processes (BP), and cellular elements (CC). The KEGG study amalgamated gene activities into a larger genomic framework. The evaluations were performed utilizing the “clusterProfiler” (4.12.3) and “GOplot” (1.0.2) software packages.<sup>19,20</sup> GO terms and KEGG pathways that had a revised *P*-value below 0.05 were deemed to have statistical significance.

## Weighted Gene Co-Expression Network Analysis (WGCNA)

The technique of Weighted Gene Co-Expression Network Analysis (WGCNA) was employed to pinpoint gene modules that show significant interrelation. Version 1.72.5 of the “WGCNA” software determines the soft threshold power ( $\beta$ ) via the “PickSoftThreshold” feature, opting for the optimal value.<sup>21</sup> Gene modules were identified using methods of weighted correlation analysis and hierarchical clustering. Every module, represented as a segment of a clustering tree, was assigned unique color codes. Disease-related modules exhibiting significant regulatory fluctuations were identified for detailed correlation analysis.

## Protein–Protein Interaction (PPI) Network Construction

PPI networks of DEGs were constructed using the STRING database (<https://cn.string-db.org/>).<sup>22</sup> Hub genes within the PPI network were identified using the CytoHubba plugin in Cytoscape through the application of four established algorithms: Degree, Edge Percolation Centrality (EPC), Maximal Clique Centrality (MCC), and Maximum Neighborhood Component (MNC).<sup>23</sup> Within each algorithm, the leading 15 core genes were chosen, and the intersection of central genes pinpointed by these four techniques was visually represented using Venn diagrams.

## Screening Hub Genes Using Machine Learning Approaches

Three distinct machine learning algorithms were employed to identify key genes associated with AF triggered by SD in GSE79768 dataset. Our response variable was the presence or absence of atrial fibrillation status, specifically a dichotomous variable: patients with atrial fibrillation were labeled as 1 and non-atrial fibrillation individuals were labeled as 0. The research utilizes the Support Vector Machine (SVM) algorithm for improving the classification precision of multi-dimensional data, employing the R package “e1071” (version 1.7.14). SVM is celebrated for their proficiency in pinpointing ideal hyperplanes for dividing data in multi-dimensional environments, and their kernel functions are particularly adept at tackling nonlinear issues.<sup>24</sup> For enhancing the model’s efficiency, a ten-fold cross-validation method was employed to equilibrate precision and error frequencies among feature variables, thereby identifying the most suitable subset of features. The “glmnet” package (version 4.1.8) in R was employed for LASSO regression analysis to execute L1 regularization, enhancing the precision of predictions and the ability to select features. This method proves especially efficient in tackling the issues of multicollinearity and dimensionality in extensive gene and PPI network data. Utilizing a three-fold cross-validation method, the mean square error was reduced to identify the ideal  $\lambda$  value, guaranteeing strong model efficacy and accurate feature choice.<sup>25</sup> Additionally, the “randomForest” package (version 4.7.1.1) in R was employed to create a Random Forest model, boosting the strength and dependability of forecasts. Random Forest, a collective learning approach utilizing decision trees, adeptly handles nonlinear data and feature interplays, simultaneously offering an inherent ranking of feature significance.<sup>26</sup> To pinpoint the most predictive

genes, a benchmark of 1 was established for feature importance scores, guaranteeing peak model efficiency and dependable feature choice. By graphing the Wayne diagrams, we identified the shared genes among the trio of machine learning algorithms.

## Validation of Hub Genes Expression

Identified hub genes were validated using the GSE79768 and GSE98582 datasets. To evaluate diagnostic value, ROC curves were generated for the training sets (GSE79768 and GSE98582) and the validation sets (GSE41177 and GSE56931), with diagnostic accuracy assessed by the area under the curve (AUC).<sup>27</sup>

## Immune Cell Infiltration Analyses

The CIBERSORT method evaluated immune infiltration profiles of 22 immune cell types in AF and control samples from the GSE79768 dataset, with  $p < 0.05$  considered significant.<sup>28</sup> Comparative analysis of immune cell distributions between AF and control groups was performed using the Wilcoxon test and “ggplot2” package (version 3.5.1). Pearson correlation analysis, visualized via the “pheatmap” package (version 1.0.12), examined the relationship between hub genes and immune cell types.

## Experimental Design and Animal Models

This research utilized Sprague-Dawley rats, ranging in age from 6 to 8 weeks and weighing between 290 and 310 g. Animals were sourced from Xinjiang Medical University’s Laboratory Animal Center and kept in a Specific Pathogen-Free environment for a week-long acclimatization phase before experimentation. Post-acclimatization, the rats were arbitrarily split into two clusters, each comprising six subjects: control group and SD group. The SD model was induced using a modified multi-platform water tank method.<sup>29</sup> Six cylindrical platforms (6.5 cm in diameter, 8 cm in height) were placed in a glass water tank, with the distance between platform centers approximately 10 cm. Adjustments were made to the water level to be 1 cm beneath the platform tops, guaranteeing that during the rats’ sleep attempts, some parts of their bodies would be immersed, leading to their awakening and subsequent lack of sleep. To satisfy the fundamental physiological requirements of the rats, they were supplied with food and water atop the tank, facilitating their unrestricted movement across platforms. For acclimatization to the tank setting, the rats were positioned on the platforms for two hours each day during the initial three days of the study. Subsequent to this adjustment, a three-day period of uninterrupted sleep deprivation was carried out.

## Experiments in Cardiac Electrophysiology

Following the successful assembly of the model, every rat was subjected to cardiac electrophysiology tests, adhering to the lab’s established protocols for anesthesia, thoracotomy, and controlled electrical stimulation.<sup>30</sup> To ascertain the Atrial Effective Refractory Period (AERP), the output voltage of the pacemaker was adjusted to double the pacing threshold. Utilizing the S1S2 decremental stimulation method, an initial interval of 200 ms was set for S1S1 and 120 ms for S2, maintaining an 8:1 stimulation ratio (S1). The duration of the S2 interval was reduced in steps of 10 ms until S1 was unable to initiate S2 conduction, and the most extended S1S2 interval where conduction halted was termed the AERP. Using the Burst stimulation technique, the rate of AF induction was gauged by adjusting the S1S1 frequency to 50 hz, with each stimulation enduring 10 seconds and replicated 10 times for each rat. The speed and diversity of conduction were documented through a microelectrode array (MEA) setup, entailing the application of a pliable MEA electrode array with 36 electrodes onto the left atrial appendage.<sup>31</sup> Following the stabilization of unipolar electrical signals by the MEA system, we produced conduction maps and determined the conduction heterogeneity index through the coefficient of variation in conduction velocity.

## Examination of Echocardiography

After a three-day span of lacking sleep, the rats underwent mild anesthesia using 1.5% isoflurane. The Vevo 2100 echocardiography system was utilized to assess their heart’s structure and functionality. The measurements encompassed left atrial diameters, left ventricular ejection fraction, and fractional shortening, averaged across three heart cycles.

## Histopathological Staining and ELISA Measurement

Rat left atrial tissue samples were first dehydrated, stabilized, encased in paraffin, cut, prepared, dewaxed, and rehydrated. Subsequently, the sections underwent staining with a Hematoxylin-eosin (HE) kit (Solarbio, No. G1120), employing hematoxylin for nucleic acid staining and eosin for cytoplasm and extracellular matrix staining. Following the staining process, the samples underwent dehydration, purification, and sealing. Following this, the tissue's morphological composition was examined using a microscope (Olympus, Tokyo, Japan). Levels of interleukin 18 (IL-18) (Jianglai biological, No. JL20882), interleukin 1 $\beta$  (IL-1 $\beta$ ) (Jianglai biological, No. JL20884), and nuclear factor  $\kappa$ B (NF- $\kappa$ B) (Jianglai biological, No. JL21039) in the serum were measured among various groups using ELISA kits, adhering to the guidelines provided by the manufacturer. Absorbance measurements were taken at 450 nm with a microplate reader, and a standard curve was derived from the collected data. Subsequently, the levels of the specified molecules in the samples were determined by applying the standard curve.

## Immunofluorescence Staining

The atrial myocardial tissue underwent dehydration, was encased, and then sliced into slices measuring 4  $\mu$ m. To maintain the stability of the tissue structure, the sections underwent fixation at 65°C for two hours, followed by deparaffinization with xylene and rehydration using a series of alcohol concentrations. The process of antigen recovery involved warming the sections using citrate buffer (Proteintech, No. PR30001). For reducing indiscriminate binding, the samples were treated with goat serum (Beyotime, No. C0265) for half an hour and left to incubate overnight at 4°C using anti-YBX1 (1:50, Beyotime, No. AF5342). After incubating with the primary antibody, a diluted secondary antibody (Proteintech, No. SA00013-2) at a ratio of 1:300 was administered, followed by a 1-hour incubation at 37°C for the creation of antibody-antigen complexes. Ultimately, the samples were prepared using a DAPI-containing anti-fading medium (Beyotime, No. P0131), and their fluorescence visuals were recorded with a Nikon fluorescence microscope. The analysis of fluorescence intensity quantitatively was conducted utilizing ImageJ software (version 1.8.0).<sup>32</sup>

## Western Blot Analysis

Protein specimens were isolated from rat atrial tissues and isolated using SDS-PAGE electrophoresis. Subsequently, the isolated proteins were relocated onto a PVDF membrane (Merck, No. C3117). To reduce indiscriminate binding, the membrane underwent blocking using 5% skim milk powder (Biosharp, No. BS102). Post-blocking, it was left to incubate overnight at 4°C with primary antibodies aimed at Nlrp3 (1:1000, Sigma, No. SAB5700723), ASC (1:1000, Abcam, No. ab309497), Caspase-1 (1:1000, Abcam, No. ab179515), YBX1 (1:1000, Beyotime, No. AF5342), and GAPDH (1:1000, Abcam, No. ab8245) serving as the internal standard. Subsequently, the membranes underwent a cleansing process using TBST buffer (Solarbio, No. T1082) to eliminate any unattached antibodies. Following this, they were subjected to a 1-hour room temperature incubation with the respective secondary antibodies to create stable antibody-antigen complexes. The identification of specific proteins utilized an ECL substrate (Proteintech, No. PK10001), and the eBlot Touch Imager system was employed to create signals. The protein expression levels were quantitatively assessed using the ImageJ software (version 1.8.0).<sup>32</sup>

## Statistical Analysis

All analyses were conducted using R (version 4.2.2) and RStudio (version 1.0.143), with data visualization performed using GraphPad Prism (version 8.0.2). Quantitative data following a normal distribution were expressed as mean  $\pm$  standard deviation. For pairwise comparisons between groups, *t*-tests were employed. Statistical significance was defined as a *p*-value <0.05.

## Results

### Co-Expression Genes Shared in AF and SD

The workflow of this study is depicted in Figure 1. To identify genes co-expressed in AF and SD, microarray data were sourced from the GSE79768 and GSE98582 datasets, which served as training sets. Probes lacking annotation were excluded from the

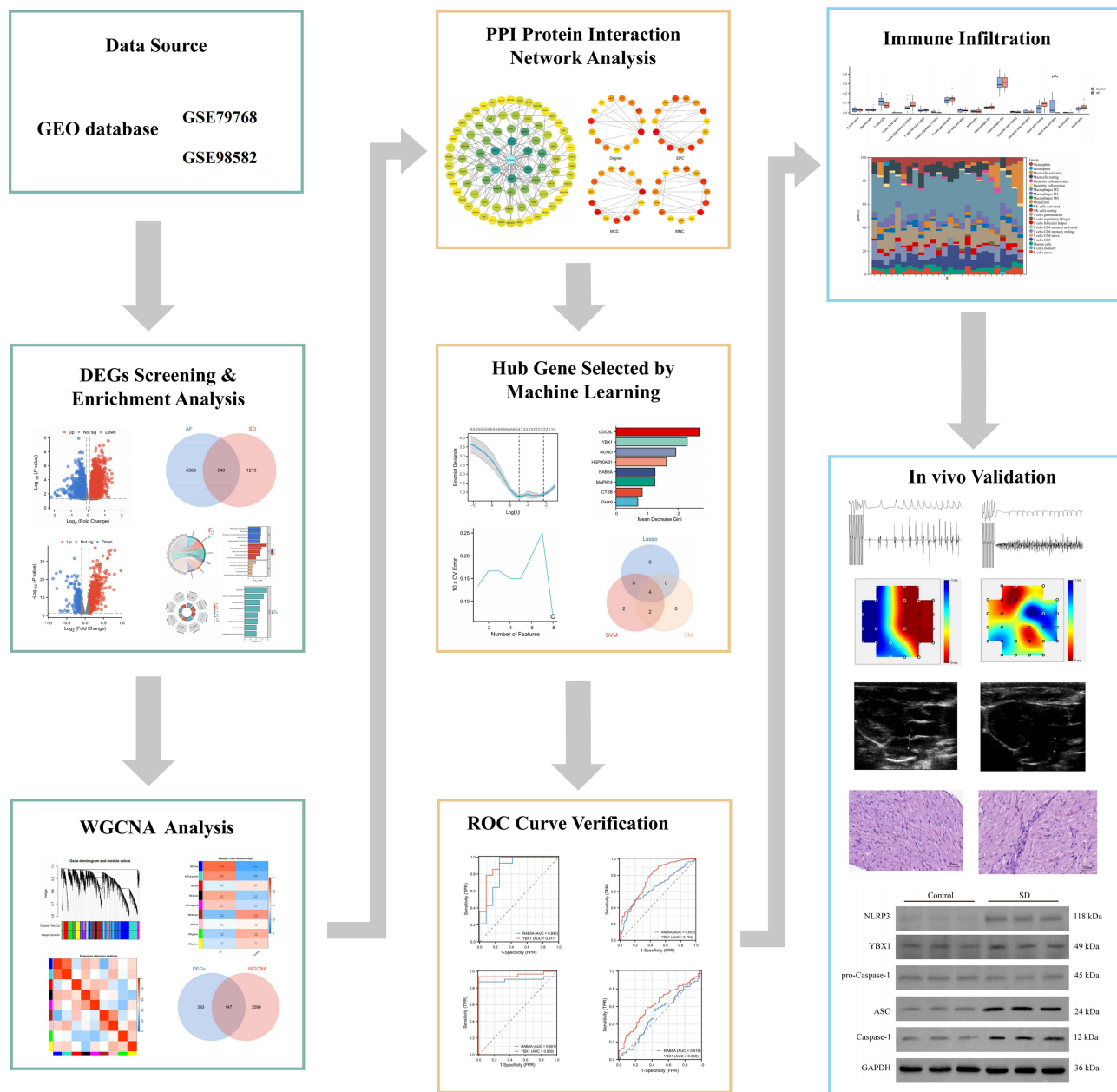


**Figure 1** Flowchart of this study.

analysis, and for genes with duplicate entries, their average expression values were computed using R software. DEGs were determined based on the criteria of  $P < 0.05$  and  $|\log_2FC| > 0.1$ . This analysis identified 6,109 DEGs in the GSE79768 dataset, including 3,317 upregulated and 2,792 downregulated genes, and 1,753 DEGs in the GSE98582 dataset, consisting of 690 upregulated and 1,063 downregulated genes. The results are illustrated through volcano plots (Figure 2A and C). Heat maps displaying the differential gene expression profiles for each dataset are provided (Figure 2B and D). Further analysis identified co-expressed genes across the two datasets using Venn diagrams (Figure 2E), indicating a possible common pathogenic mechanism underlying both AF and SD.

## Functional Enrichment Analysis of Common Genes

To further investigate the biological functions and pathways associated with the common DEGs, we conducted GO and KEGG enrichment analyses. The GO enrichment analysis revealed that the most significant biological processes (BP) involved

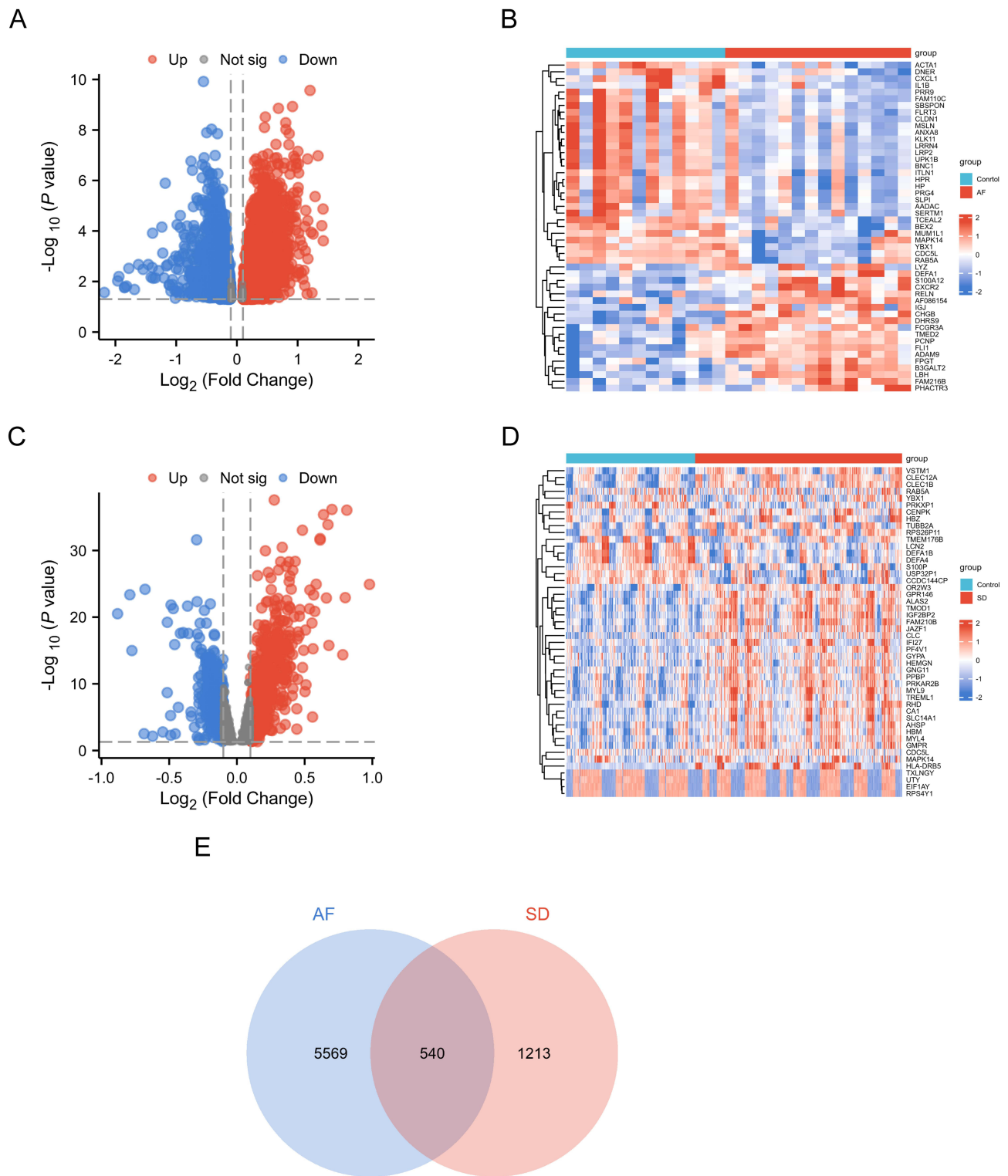


**Figure 2** Identification of DEGs associated with AF and SD. **(A)** Volcano plot illustrating DEGs from the GSE79768 dataset. **(B)** Corresponding heat map of the DEGs from the GSE79768 dataset. **(C)** Volcano plot of DEGs identified in the GSE98582 dataset. **(D)** Heat map of the DEGs from the GSE98582 dataset. **(E)** Venn diagram showing the overlap of differentially expressed genes between the conditions of SD and AF. **Abbreviations:** AF, atrial fibrillation; SD, sleep deprivation.

mRNA processing, histone modification, and RNA splicing. Regarding cellular components (CC), the genes were predominantly enriched in nuclear specks, transcription regulator complexes, and cell-substrate junctions. In terms of molecular function (MF), the key enrichments were in transcription coregulator activity, phospholipid binding, and ubiquitin-like protein transferase activity (Figure 3A and B). KEGG pathway analysis identified significant enrichment in pathways related to Salmonella infection, NOD-like receptor signaling, and the spliceosome (Figure 3C and D) (Table 2). Collectively, these findings suggest that inflammatory pathways play a crucial role in the pathogenesis of both AF and SD.

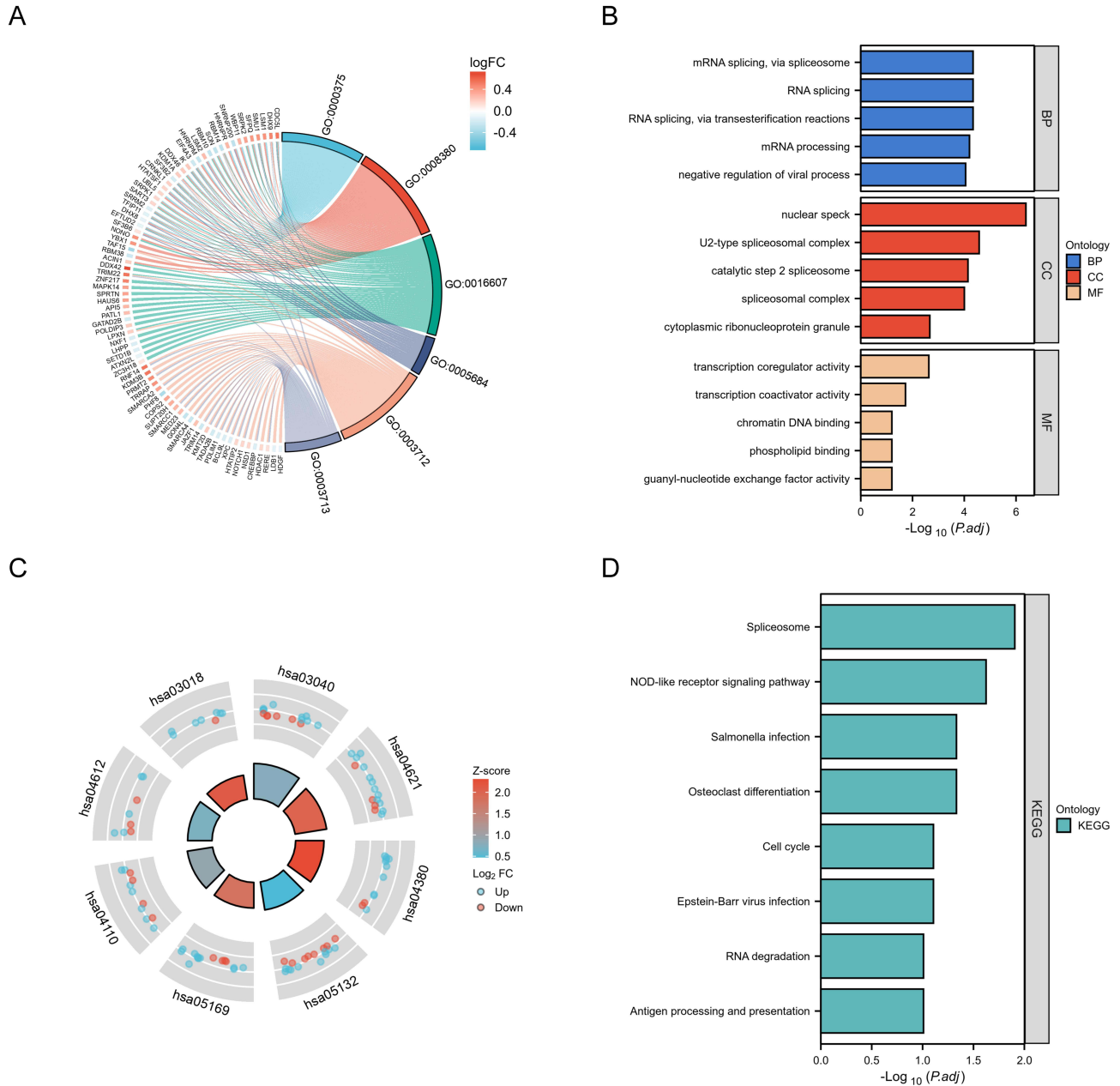


**Figure 3** Enrichment analysis of common DEGs. **(A)** Circular plot of enriched Gene Ontology (GO) terms for DEGs, with color indicating logFC. **(B)** Bar charts of the top GO terms across BP, CC, and MF, ranked by  $-\log_{10}(P\text{-adjusted})$ . **(C)** Circular heatmap of KEGG pathway enrichment, showing pathways by logFC and Z-score. **(D)** Bar chart of the top KEGG pathways, ranked by  $-\log_{10}(P\text{-adjusted})$ .

**Abbreviations:** BP, Biological Process; CC, Cellular Component; MF, Molecular Function.

**Table 2** KEGG Pathway Enrichment

ID	Description	pvalue
hsa03040	Spliceosome	4.70E-05
hsa04621	NOD-like receptor signaling pathway	1.80E-04
hsa04380	Osteoclast differentiation	5.90E-04
hsa05132	Salmonella infection	7.04E-04
hsa05169	Epstein-Barr virus infection	1.49E-03
hsa04110	Cell cycle	1.78E-03
hsa04612	Antigen processing and presentation	2.74E-03
hsa03018	RNA degradation	2.97E-03

## WGCNA Analysis

In the GSE79768 dataset, the WGCNA established a soft threshold of 4, identifying nine distinct gene modules with similar co-expression patterns. To determine the most relevant modules, we calculated the Spearman correlation coefficients between these modules and specific traits (Figures 4A–C). The blue and brown modules were identified as particularly significant due to their strong association with AF. To further explore the overlap between these target modules, a Venn diagram was employed to compare the implicated genes (Figure 4D). This analysis highlights the critical role of the blue and brown modules in understanding the genetic underpinnings of AF.

## PPI Network Construction and Hub Genes Screening via Machine Learning Approaches

In this study, we performed a comprehensive analysis of DEGs involved in both AF and SD. We initiated our investigation by constructing a PPI network of 147 DEGs using the STRING database, which was subsequently visualized and thoroughly analyzed with Cytoscape software (Figure 5A). To identify key genes within this network, we employed the CytoHubba plug-in in Cytoscape, applying four centrality algorithms: MMC, Degree, EPC, and MNC. Each algorithm was used to rank the top 15 significant genes in the network (Figure 5B). The overlapping genes identified by these algorithms were then illustrated using Venn diagrams to emphasize their shared significance (Figure 5C). Building on the PPI network findings, we employed three advanced machine learning algorithms to rigorously identify key feature genes. LASSO regression further refined this selection, identifying four critical genes from the statistically significant candidates (Figure 5D and E) (Table S1). The Random Forest algorithm pinpointed six important genes based on a significance score exceeding 1 (Figure 5F) (Table S2). Additionally, the SVM algorithm highlighted eight genes with strong predictive features, achieving a model accuracy of 0.933 and an error rate of 0.067 (Figure 5G and H) (Table S3). Through Venn diagram analysis, four genes—CDC5L, MAPK14, RAB5A, and YBX1—were consistently identified across all three algorithms (Figure 5I). The recurrent identification of these genes underscores their potential central role in the pathological processes of AF and SD, positioning them as valuable molecular markers for future biological research and clinical application.

## Validation of Hub Genes Reliability Across Datasets

To validate the reliability of four candidate hub genes, we initially assessed their expression levels in two independent training sets, GSE79768 and GSE98582. In the GSE79768 dataset, all four hub genes exhibited upregulated expression in the AF group (Figure 6A–D). However, in the GSE98582 dataset, the expression patterns were inconsistent: CDC5L and MAPK14 were downregulated in the SD group, while RAB5A and YBX1 were upregulated (Figure 6E–H). Given the discordant expression trends of CDC5L and MAPK14 between the AF and SD groups, these two genes were excluded from further analysis. We then focused on the remaining two hub genes, RAB5A and YBX1, and evaluated their

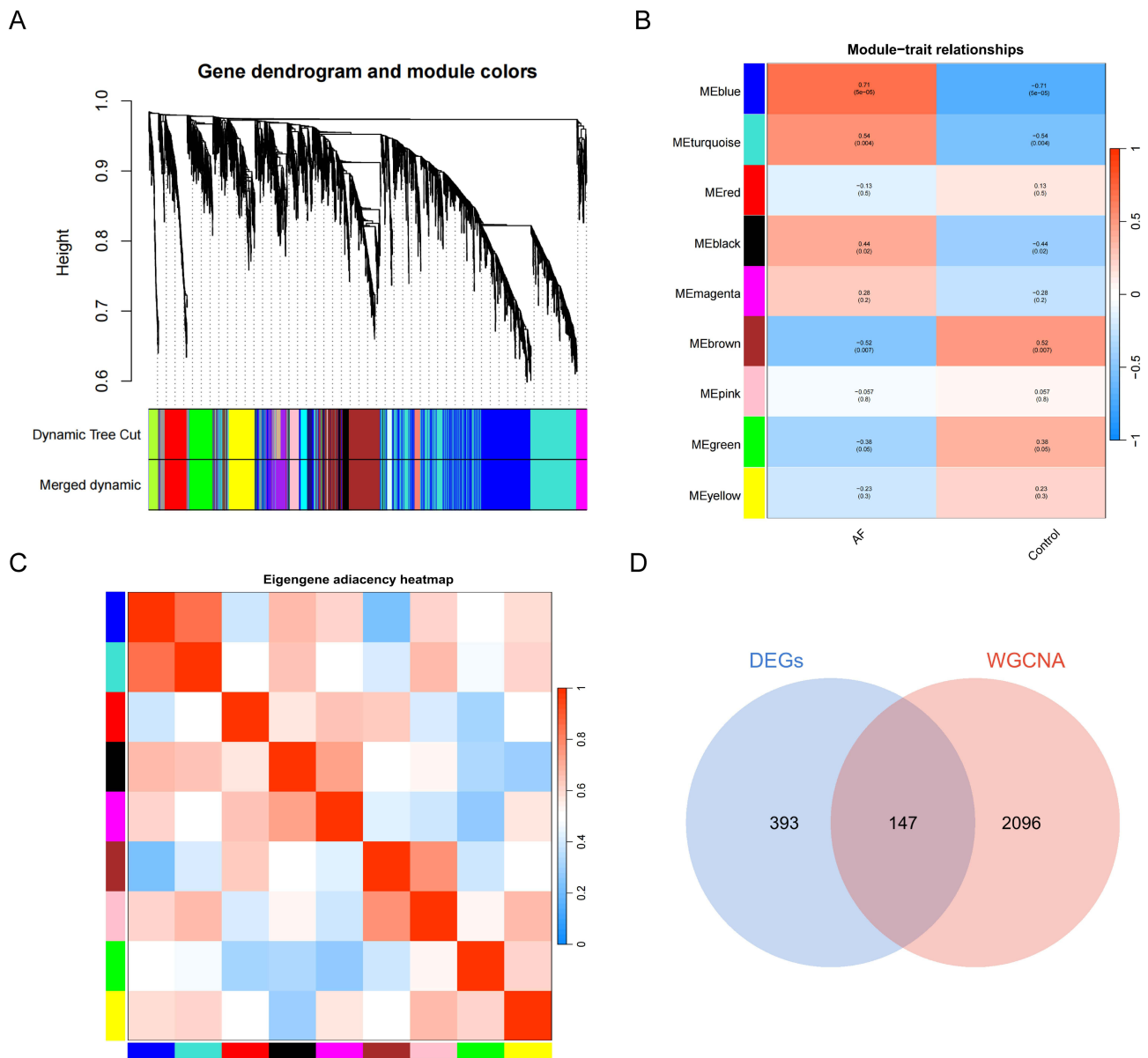


**Figure 4** Weighted Gene Co-expression Network Analysis (WGCNA) of the GSE79768 dataset and intersecting genes. **(A)** Gene dendrogram and module color assignment, generated by hierarchical clustering and dynamic tree cutting, showing modules of co-expressed genes. **(B)** Correlation heatmap of module eigengenes with AF and control traits; colors indicate the strength and direction of correlations. **(C)** Heatmap of eigengene adjacency, representing the correlations among gene modules. **(D)** Venn diagram showing the overlap between DEGs and WGCNA-identified modules, highlighting 147 shared genes.

diagnostic performance by plotting ROC curves across the training and validation sets. Notably, the AUC values for YBX1 were 0.917 and 0.764 in the GSE79768 and GSE98582 datasets, respectively, while the AUC values in the GSE56931 and GSE41177 datasets exceeded 0.6. (Figure 7A–D).

### The Correlations Between Critical Gene and Immune Cell Infiltration

To investigate the potential link between AF and immunomodulation, we employed the CIBERSORT algorithm to evaluate immune cell infiltration differences between Control and AF groups within the GSE79768 dataset. The analysis revealed significant variations in the infiltration levels of resting memory CD4+ T cells, neutrophils, and macrophages between the two groups (Figure 8A and B). These findings highlight a potentially critical role for immune cell infiltration in the pathogenesis of AF. Furthermore, we examined the relationship between central gene expression and immune cell infiltration through Pearson correlation analysis. Notably, YBX1 expression was found to be negatively correlated with

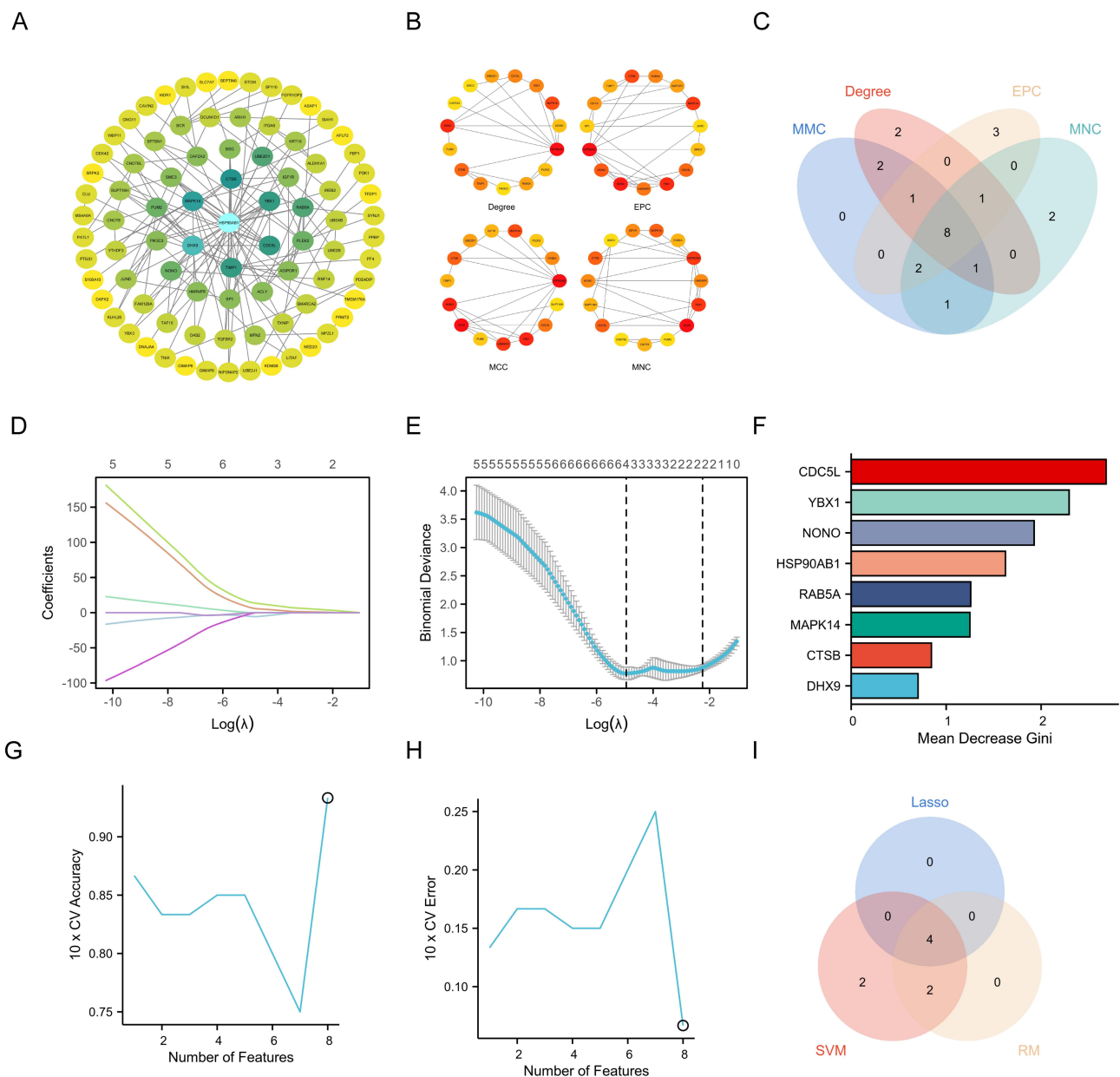


**Figure 5** Feature selection and network analysis of key genes. **(A)** Protein-protein interaction (PPI) network of key genes identified by feature selection methods. **(B)** Centrality analyses of the PPI network using degree, EPC, MCC, and MNC metrics. **(C)** Venn diagram showing the overlap of top genes identified by different centrality measures. **(D)** Lasso regression coefficient profiles for gene selection across varying  $\log(\lambda)$  values. **(E)** Binomial deviance plot for Lasso regression, with vertical dashed lines indicating the optimal  $\lambda$ . **(F)** Top genes ranked by the mean decrease in Gini index from random forest analysis. **(G and H)** Plots of 10-fold CV accuracy and error versus the number of selected features. **(I)** Venn diagram depicting the overlap of key genes identified by Lasso, SVM, and RF models.

**Abbreviations:** CV, cross-validation; SVM, support vector machine; RF, random forest.

CD8<sup>+</sup> T cells and M1 macrophage infiltration (Figure 8C–E). This suggests that YBX1 may play a role in the immunoregulatory mechanisms of AF by modulating the activity and function of specific immune cells, thereby potentially contributing to the pathological processes underlying AF.

## SD Increases Atrial Electrical Remodeling

In this study, we investigated the impact of SD on atrial electrical remodeling in a rat model. Using in vivo programmed electrical stimulation, we observed that both the rate of AF induction and the duration of AF were significantly higher in the SD group compared to the Control group (Figure 9A, D and E). Additionally, the AERP was notably shortened in the

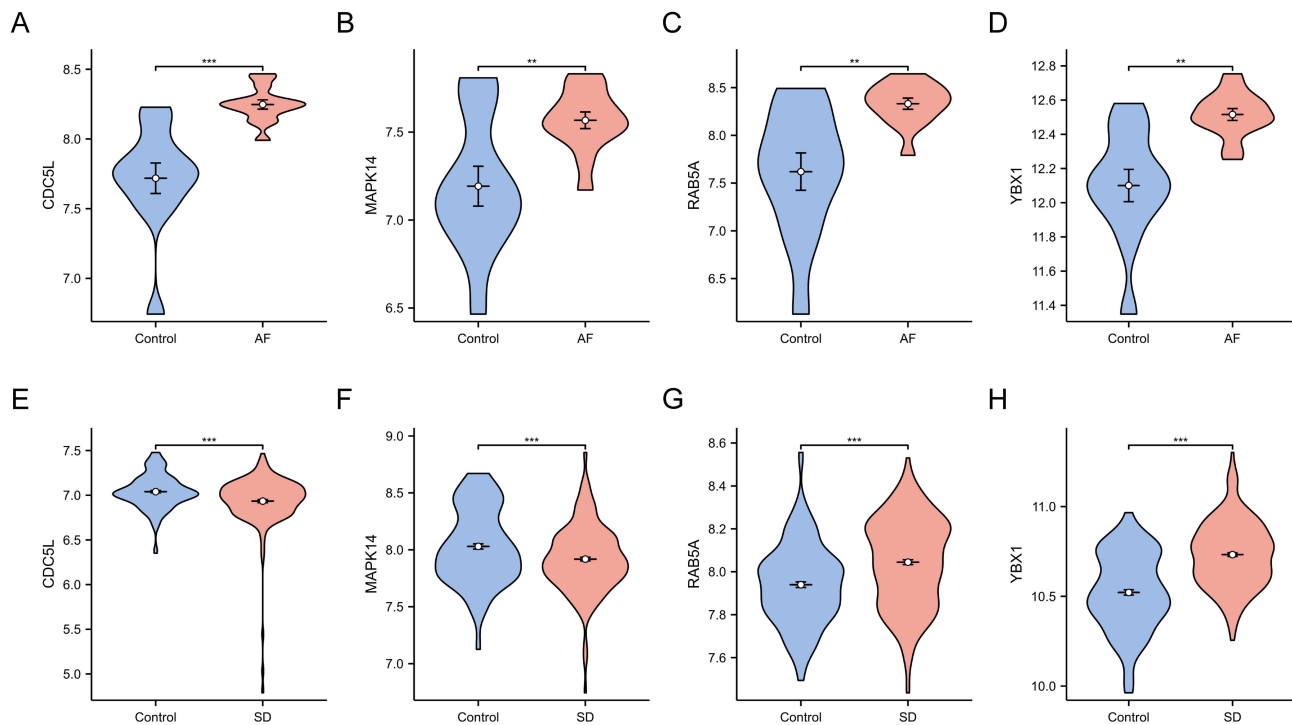


**Figure 6** Validation of key gene expression in GSE79768 and GSE98582 dataset. (A–D) Violin plots showing the expression levels of CDC5L, MAPK14, RAB5A, and YBX1 in AF versus control groups in the GSE79768 dataset. (E–H) Violin plots of the same genes comparing SD versus control groups in the GSE98582 dataset. Asterisks denote levels of statistical significance:  $P < 0.01$  (\*\*),  $P < 0.001$  (\*\*\*).

SD group (Figure 9C). Moreover, MEA analysis revealed significant disruptions in the homogeneity and orderliness of atrial electrical conduction in the SD group (Figure 9B). There was an increased frequency of ectopic activation points, a significant elevation in the inhomogeneity index, and a marked reduction in conduction velocity compared with the control group (Figure 9F and G). These findings suggest that SD may promote atrial electrical remodeling by altering atrial electrophysiological properties, thereby contributing to the pathogenesis of AF.

## SD Increases Atrial Structural Remodeling

In this study, we employed cardiac color ultrasound and HE staining techniques to comprehensively evaluate the cardiac structure and function in a rat model, with the objective of investigating the impact of SD on atrial myocardial architecture and cardiac performance. Cardiac ultrasound results revealed a significant dilation of the left atrium in rats subjected to SD, though no notable changes in overall cardiac function were observed (Figure 10A, B, D and H). Analysis using HE staining revealed that the myocardial fibers in the control group displayed a structured arrangement, maintaining consistent morphology and unaltered architecture. In contrast, the SD group's myocardial tissue exhibited notable disarray and significant infiltration of inflammatory cells (Figure 10C). Additionally, ELISA tests revealed a marked increase in serum concentrations of IL-1 $\beta$ , IL-18, and NF- $\kappa$ B in the SD group relative to the control group (Figure 10E–G). The results indicate that SD could undermine the structural soundness of atrial tissue through the stimulation of pro-inflammatory cytokines release and the intensification of inflammatory cell penetration, collectively leading to the onset of pathophysiological alterations in atrium.

## Validation of Hub Gene and Potential Pathway

Our research into YBX1 expression in SD-related AF and the investigation of possible foundational pathways employed immunofluorescence and Western blotting methods to measure pertinent molecular indicators. The immunofluorescence study we conducted showed a marked rise in the intensity of YBX1 fluorescence in the cardiomyocytes of rats exposed to

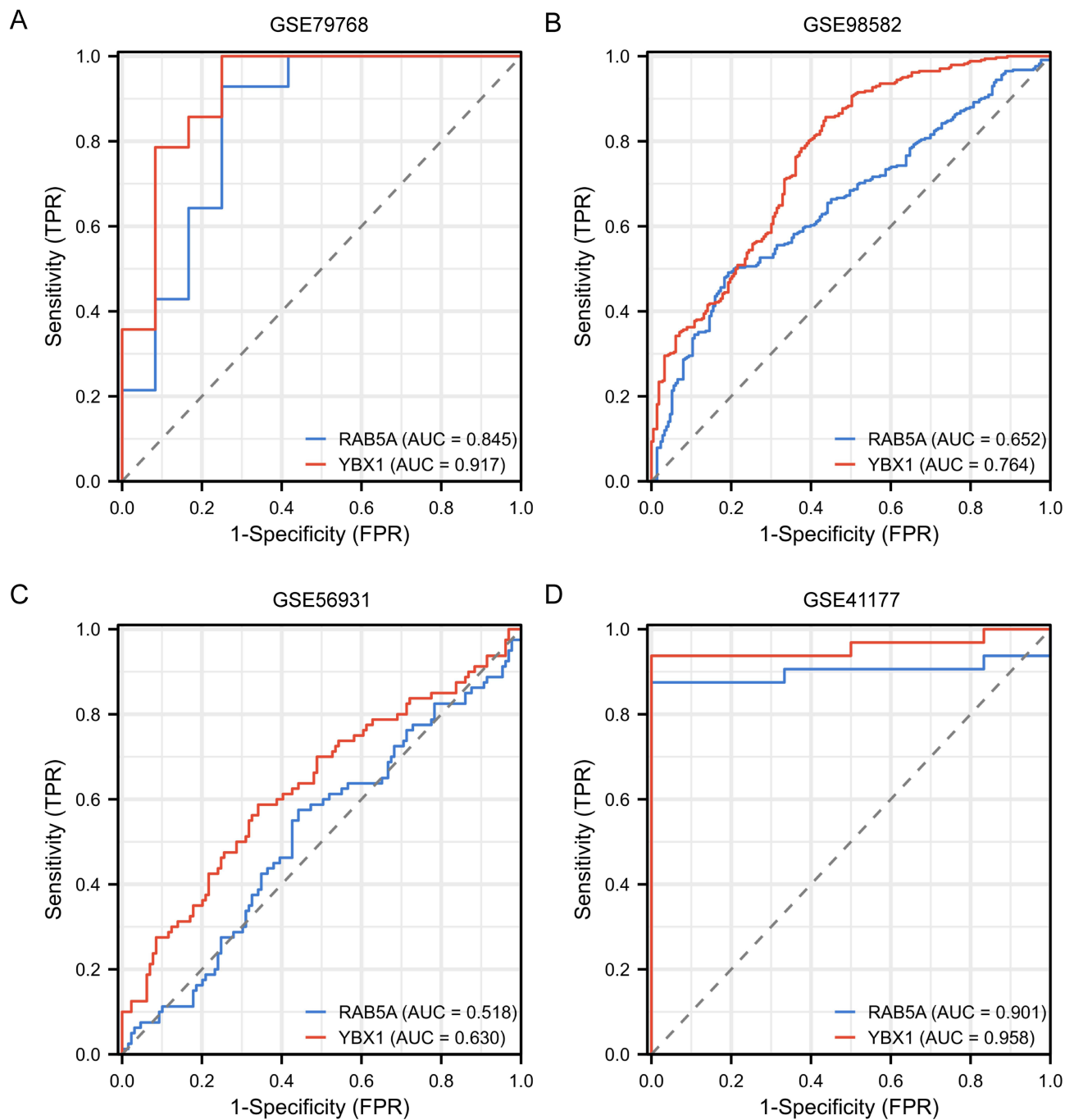


**Figure 7** ROC curves for key genes across multiple datasets. (A–D) ROC curves illustrating the diagnostic performance of RAB5A and YBX1 in distinguishing cases from controls in datasets GSE79768 (A), GSE98582 (B), GSE56931 (C), and GSE41177 (D). The x-axis represents the false positive rate (1-Specificity), and the y-axis represents the true positive rate (Sensitivity). Blue lines represent RAB5A, red lines represent YBX1, and the dashed diagonal line indicates random performance (AUC=0.5).

**Abbreviations:** ROC, receiver operating characteristic; AUC, area under the curve.

SD, signifying a marked increase in YBX1 expression in these circumstances (Figure 11A and C). Simultaneously, Western blot analysis supported these results, revealing increased amounts of NLRP3, ASC, Caspase-1, and YBX1 proteins in the heart muscle tissues of SD rats (Figure 11B, D–H). These proteins play a vital role in the inflammasome pathway, and their increased expression indicates a link to myocardial inflammation triggered by SD.

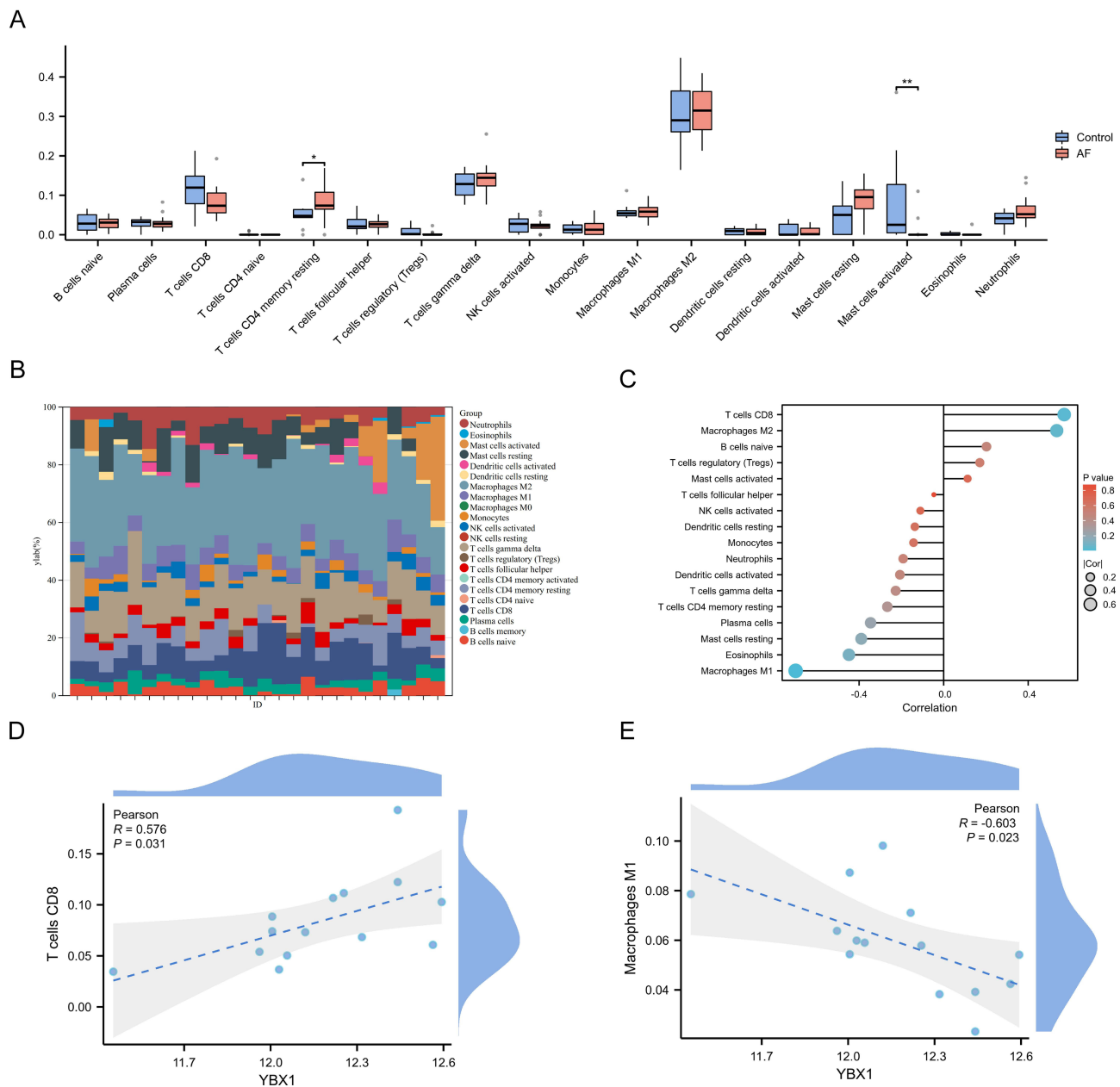


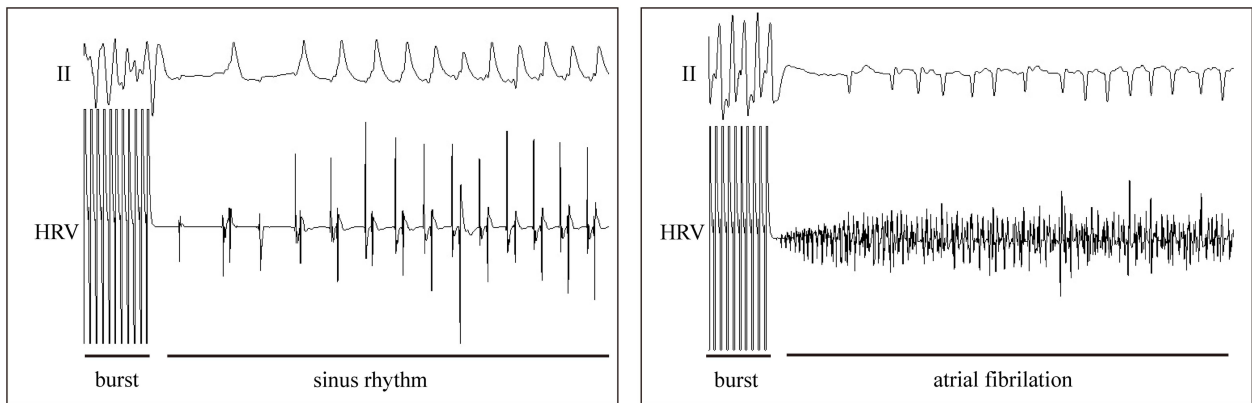
**Figure 8** Immune infiltration analysis and correlation of YBX1 expression with immune cell populations in the GSE79768 dataset. **(A)** Box plots showing the relative proportions of various immune cell types in AF versus control groups. **(B)** Stacked bar chart representing the composition of immune cells in individual samples. **(C)** Correlation analysis of YBX1 expression with different immune cell populations, with size and color of dots indicating correlation coefficients and p-values, respectively. **(D and E)** Scatter plots illustrating the correlations between YBX1 expression and the abundance of CD8+ T cells **(D)** and M1 macrophages **(E)**, with Pearson correlation coefficients and p-values displayed. Asterisks denote statistically significant differences:  $P < 0.05$  (\*),  $P < 0.01$  (\*\*).

## Discussion

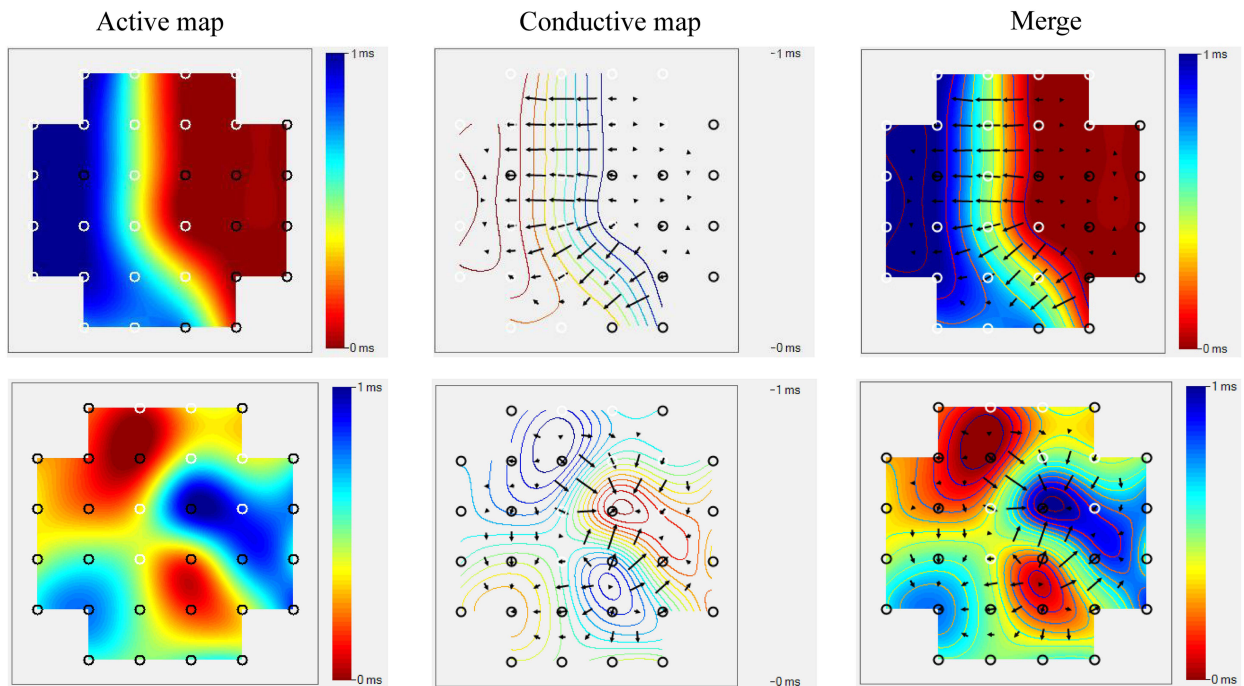
AF stands as the most common type of cardiac arrhythmia, impacting millions worldwide and playing a major role in escalating morbidity and mortality rates.<sup>33</sup> SD has emerged as a critical risk factor for various cardiovascular diseases, including AF.<sup>34</sup> Considering the prevalent presence of SD in modern society, comprehensively grasping its effects on AF is crucial for developing successful prevention and management approaches.

This research presents crucial discoveries: SD significantly increases the risk of AF; YBX1 is recognized as a key gene linked to AF caused by sleep deprivation; and the NOD-Like Receptor signaling pathway plays a vital role in the development of AF associated with SD. Furthermore, our findings indicate that SD markedly reduced the AERP in rats,

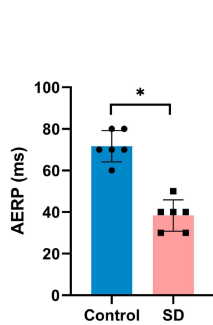
A



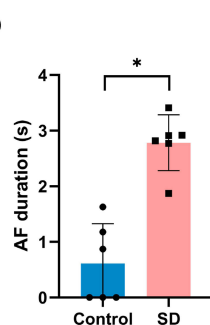
B



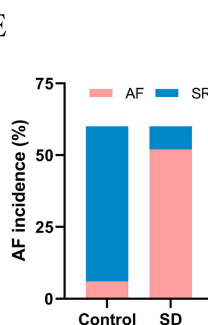
C



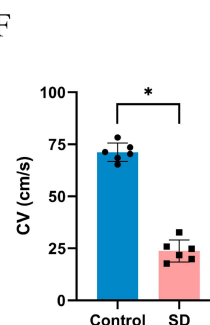
D



E



F



G

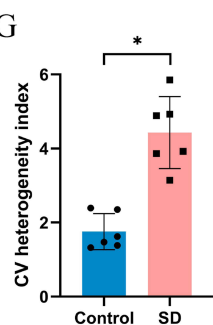


**Figure 9** Increased susceptibility to AF in rats following SD. **(A)** Representative ECG recordings showing sinus rhythm and AF induction in control and SD groups. **(B)** Electrophysiological mapping displaying activation maps, conduction velocity maps, and merged maps for both groups. **(C)** Bar graph showing AERP in control and SD groups. **(D)** Duration of AF episodes in both groups. **(E)** AF incidence rates in control and SD groups. **(F)** CV comparison between groups. **(G)** CV heterogeneity index in control and SD groups. Asterisks denote statistical significance:  $P < 0.05$  (\*). **Abbreviations:** AERP, atrial effective refractory period; CV, conduction velocity; SR, sinus rhythm.

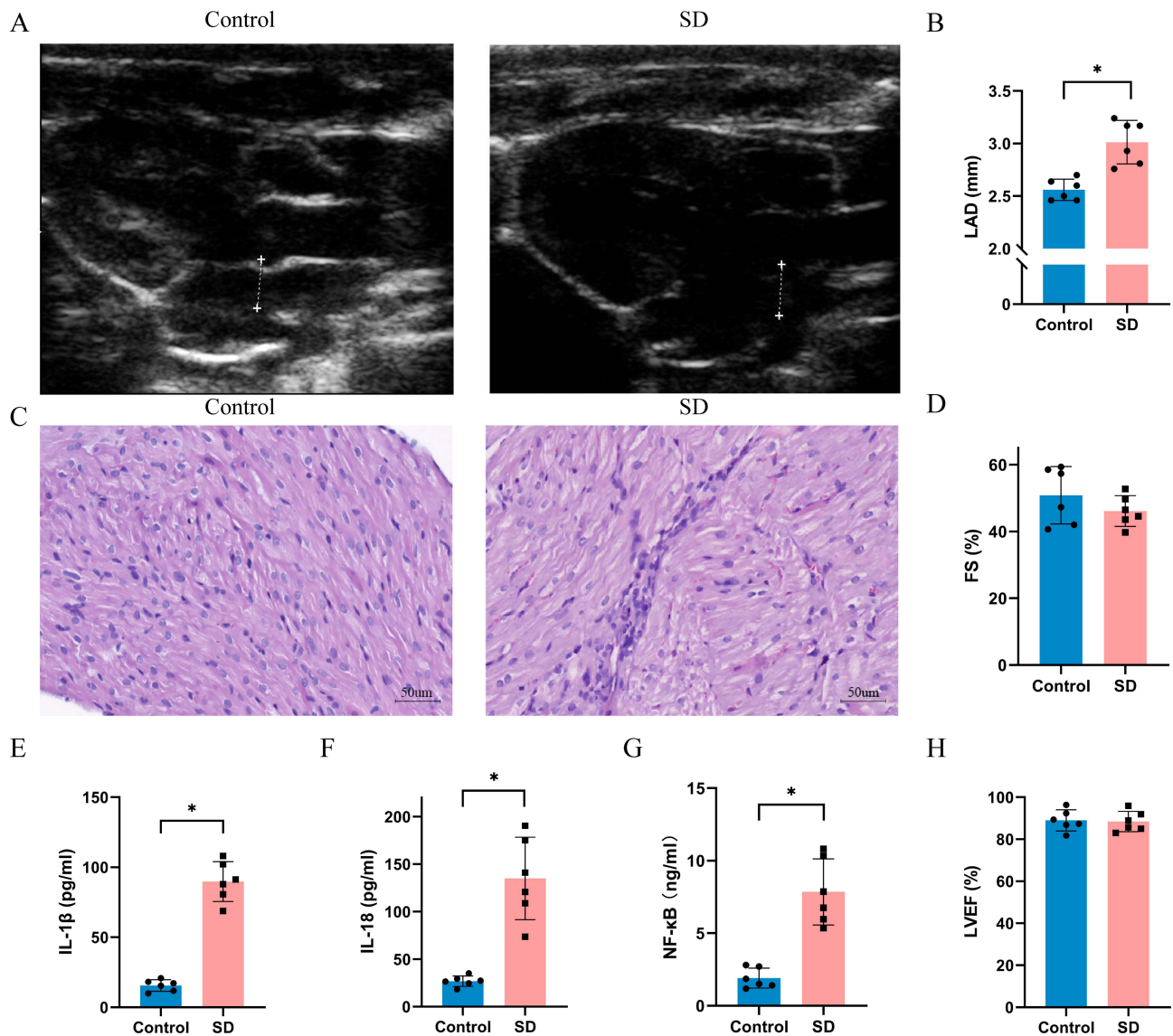


**Figure 10** Echocardiographic, histopathological, and biochemical assessment in control and SD groups. (A) Representative cardiac ultrasound images showing LAD in control and SD rats. (B) Quantification of LAD in both groups. (C) HE staining of cardiac tissue showing histopathological differences between control and SD groups. Scale bars: 50  $\mu$ M (D) LVFS comparison between groups. (E–G) ELISA quantification of inflammatory markers, including IL-1 $\beta$  (E), IL-18 (F), and NF- $\kappa$ B (G) levels in cardiac tissue. (H) LVEF comparison between groups. Asterisks indicate statistical significance:  $P < 0.05$ (\*).

**Abbreviations:** HE, Hematoxylin and eosin; LAD, left atrial diameter; FS, fractional shortening; LVEF, Left ventricular ejection fraction; IL-1 $\beta$ , interleukin 1 $\beta$ ; IL-18, interleukin 18; NF- $\kappa$ B, nuclear factor  $\kappa$ B.

and markedly prolonged the induction and duration of AF, along with the inflammatory invasion of atrial tissue. The alterations observed aligned closely with the pathological processes of human AF, primarily regarding the electrical and structural remodeling of the atria. The findings reinforce the significance of the SD rat model in mimicking the development of human AF and offer a dependable animal model for comprehensive research into AF's pathogenesis. The results of this research are depicted in Figure 12.

This research began by pinpointing crucial genes associated with both SD and AF, followed by a thorough examination to clarify the possible pathogenic links between these two disorders. By analyzing the datasets GSE79768 and GSE98582, 540 shared genes were pinpointed. Subsequently, we utilized WGCNA, PPI analysis, and various machine learning techniques such as Random Forest, Support Vector Machines, and LASSO regression to identify four crucial genes: CDC5L, MAPK14, RAB5A, and YBX1. The gene expression intensities were additionally corroborated using datasets pertinent to both SD and AF. The results of our study showed that the expression of CDC5L and MAPK14

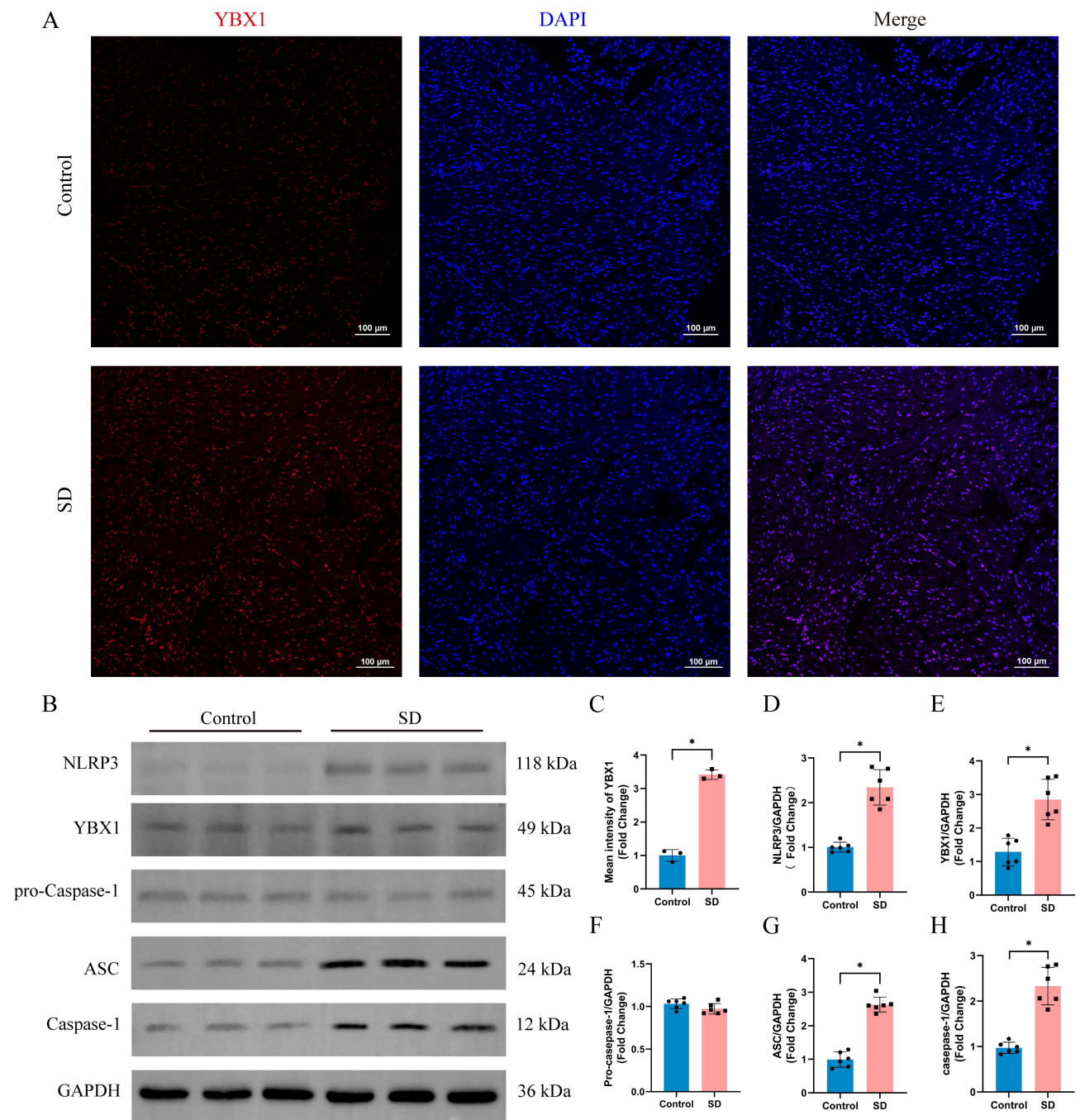


**Figure 11** Expression analysis of YBX1 and key molecules in the NOD-like receptor signaling pathway. **(A)** Representative immunofluorescence images showing YBX1 (red) localization in myocardial tissue, counterstained with DAPI (blue) in control and SD groups; merged images demonstrate co-localization. Scale bars: 100  $\mu$ M **(B)** Western blot analysis of NLRP3, YBX1, pro-caspase-1, ASC, and caspase-1 in cardiac tissue from control and SD groups, with GAPDH as the loading control. **(C)** Quantification of YBX1 fluorescence intensity, showing increased expression in the SD group compared to control. **(D–H)** Quantification of protein expression levels of NLRP3 **(D)**, pro-caspase-1 **(F)**, ASC **(G)**, and active caspase-1 **(H)** relative to GAPDH, indicating upregulation in the SD group. Asterisks denote statistically significant differences:  $P < 0.05$ (<sup>\*</sup>).

varied between SD and AF, resulting in their omission from additional analysis. ROC curve analysis was applied to the last two genes, RAB5A and YBX1, revealing YBX1's significant diagnostic utility in various datasets. Furthermore, the analysis of immune infiltration revealed a positive association between YBX1 expression and CD8<sup>+</sup> T cells, while showing a negative correlation with M1 macrophage infiltration. The findings emphasize YBX1's crucial function in the development of SD-related AF and underscore its connection to immune cell penetration.

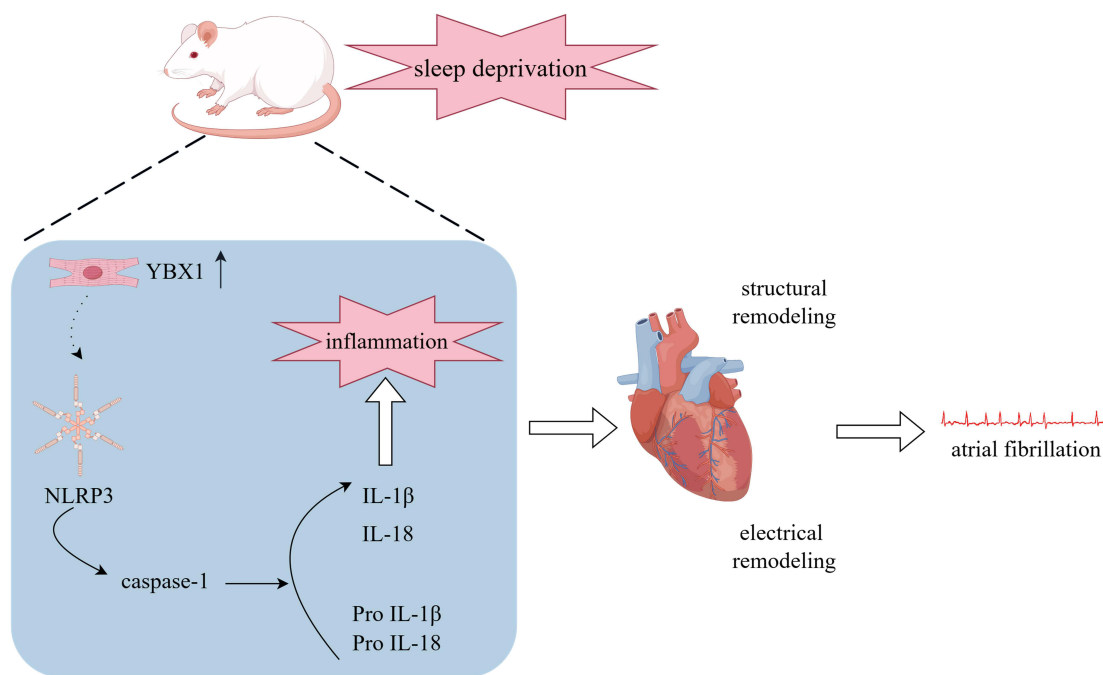


**Figure 12** Schematic diagram of the study. Sleep deprivation increases susceptibility to atrial fibrillation by upregulating YBX1 and activating the NLRP3 inflammasome.

The protein YBX1, known as Y-box binding protein 1, binds to DNA and RNA and is distinguished by its extensively preserved cold shock domain.<sup>35</sup> This element plays a role in numerous cellular activities such as transcription, translation, and repairing DNA damage, and its expression increases when exposed to environmental stressors.<sup>36</sup> YBX1 plays a pivotal role in controlling the cardiovascular and immune systems. In vascular remodeling, YBX1 acts as a crucial transcription factor, with its movement within the nucleus and ability to bind chromatin controlled by LncRNA PSRs, facilitating phenotypic changes in vascular smooth muscle cells and initiating pathological vascular alterations.<sup>37</sup> Throughout pathological myocardial restructuring, the mTOR signaling route regulates YBX1, accelerating protein synthesis through increased eEF2 translation, thereby aiding in pathological myocardial expansion.<sup>38</sup> Furthermore, inhibiting YBX1 enhances cardiomyocyte efficiency and assists in recuperating from post-myocardial infarction.<sup>39</sup> YBX1 is a critical regulator of the immune system, influencing multiple stages of immune responses. As an essential antigenic molecule, YBX1 significantly amplifies T-cell immune reactions, particularly in the context of Treg cell suppression, due to its potent immune-activating properties.<sup>40,41</sup> This enhancement of cellular immunity leads to increased antigen detection and the strengthening of protective immune responses. Furthermore, YBX1 exhibits cell-type specificity in cytokine regulation; it reduces mRNA levels within macrophages through vesicular transport, while maintaining mRNA stability in dendritic cells.<sup>42</sup> The current research pinpointed YBX1 as a key gene linked to sleep deprivation-related atrial fibrillation. In vivo experiments revealed a notable increase in YBX1 levels in the group experiencing sleep deprivation, indicating its possible involvement in regulating the stress response and inflammation of cardiomyocytes.

This study pinpointed shared differential genes in SD and AF, and later GO and KEGG enrichment studies showed a notable increase in the NOD-Like Receptor signaling pathway. This route is essential for internal cellular communication, crucially involved in identifying pathogens and responding to the innate immune system.<sup>43</sup> The NLRP3 inflammasome, a crucial part of the NOD-like receptor family, is made up of three primary elements: NLRP3, ASC, and caspase-1, and exhibits a heightened sensitivity to internal threat signals. The activation process encompasses various cellular signaling routes, including the expulsion of potassium ions, creation of mitochondrial reactive oxygen species, and lysosomal rupture, collectively facilitating the development and release of IL-1β and IL-18. The pair of pro-inflammatory cytokines are pivotal in controlling the combined impact of innate and adaptive immunity, amplifying the inflammatory reaction via the pyroptosis route.<sup>44</sup> Furthermore, NLRP3 alters the unconventional secretion process of IL-1α via distinct signaling pathways in Th17 cells, thereby amplifying its pro-inflammatory characteristics.<sup>45</sup> This layered regulatory process of NLRP3 plays a crucial role in sustaining immune balance and

lays the groundwork for creating strategies for immune intervention. The NLRP3 inflammasome plays a crucial role in the development of cardiovascular disorders. The influence they have on the emergence and progression of diseases is significant, initiating inflammatory responses and routes that result in programmed cellular demise. Specifically, the NLRP3 inflammasome escalates inflammation by triggering the release of IL-1 $\beta$  and IL-18, both of which are linked to the formation of unstable plaques in atherosclerosis.<sup>46</sup> Furthermore, elevated levels of lipopolysaccharides, due to a disruption in gut flora, can initiate the NLRP3 inflammasome, leading to the emergence and persistence of AF.<sup>47</sup> Inhibiting the NLRP3 inflammasome and its ensuing effects has shown promising outcomes in numerous studies. The CANTOS research indicated that inhibitors of IL-1 $\beta$  significantly reduced the risk of adverse cardiovascular events in patients with atherosclerosis, whereas the NLRP3-focused inhibitor MCC950 effectively curtailed atrial fibrillation and myocardial fibrosis in animal studies.<sup>46,47</sup> The results of our study reveal that lack of sleep triggers the NLRP3 inflammasome, leading to both electrical and structural alterations in the atria. Earlier research has also shown a strong link between the activation of NLRP3 inflammasomes and the electrical and structural changes in the atrium, indicating that this activation might play a role in the emergence of AF.<sup>48</sup> This effect can manifest via multiple pathways, encompassing changes in the electrophysiological characteristics of cardiomyocytes, the release of calcium from the sarcoplasmic reticulum, the period of atrial effective refractory, and the enlargement of the atrium.<sup>49</sup> Therefore, it appears logical to propose that insufficient sleep might affect the electrical and structural properties of the atria by enhancing the function of the NLRP3 inflammasome, leading to a rise in AF rates.

Our research indicated a positive association between the expression of the target molecule YBX1 and CD8+ T cells, and a negative one with M1-type macrophages, highlighting the significant function of immune cells in SD-related AF. Previous studies have shown that the immune response plays a key role in AF and SD, especially T-cell activation and macrophage polarization. CD8+ T cells cause direct harm to cardiomyocytes and initiate inflammation by releasing proinflammatory elements like IFN- $\gamma$  and cytotoxic substances such as perforins and granzymes.<sup>50,51</sup> The inflammatory reaction results in irregular calcium management and electrophysiological disruptions in cardiomyocytes, elevating the likelihood of AF and its recurrence post-surgery. It also aligns with the senescent characteristics of CD8+ T cells, intensifying the diversity of atrial electrical activities and disruptions in conduction by intensifying proinflammatory actions.<sup>52</sup> Macrophages also play an important role in the pathomechanism of AF. Specific macrophage variants stimulate atrial fibroblasts by releasing pro-fibrotic elements like osteoblasts and TGF- $\beta$ , hastening the build-up of the extracellular matrix, and intensifying atrial fibrosis, leading to the persistence and advancement of AF.<sup>53,54</sup> The dual regulatory effects of sleep deprivation on the immune system are reflected in the profound effects on CD8+ T cell and macrophage function. Sleep deprivation leads to impaired CD8+ T cell function, which is manifested by decreased cell proliferation and activity, weakening the body's anti-infection and anti-virus ability.<sup>55</sup> Furthermore, Wilder-Smith A et al demonstrated that partial and complete sleep deprivation induced dynamic changes in CD8+ T-cell numbers, with a transient decrease in CD8+ T-cells after partial deprivation followed by a gradual recovery.<sup>56</sup> Macrophages also underwent significant functional changes after sleep deprivation, and in particular, the pro-inflammatory role of M1-type macrophages was enhanced, as evidenced by significant secretion of pro-inflammatory factors such as TNF- $\alpha$  and IL-1 $\beta$ . In contrast, the differentiation of M2-type macrophages and their anti-inflammatory functions were inhibited, diminishing their role in tissue repair and immunomodulation.<sup>57</sup> Macrophage function is also closely related to sleep recovery, and in a sleep deprivation model, mice with macrophage depletion or M2-type macrophage deletion had significantly reduced recovery from non-rapid eye movement sleep, confirming the important role of macrophages in sleep regulation.<sup>58</sup>

## Limitations

Although this research sheds light on the molecular connections between SD and AF, it is not without its constraints. Significantly, there is an absence of an in-depth examination of how YBX1 and NLRP3 inflammasome activation interrelate. Despite the recognition of YBX1 as a key gene in SD-related AF, its immediate function in regulating NLRP3 inflammasome activation is still not investigated. The absence of this detail hinders our comprehension of how YBX1 affects the inflammatory process in AF. Subsequent studies ought to concentrate on elucidating this link via specific experiments, potentially offering a broader insight into SD-induced AF and guiding innovative treatment approaches.

## Conclusion

The research uncovers YBX1's crucial function in connecting SD with AF, underscoring its role in inflammation processes and immune reactions. Bioinformatics and experimental studies have identified YBX1 as a crucial gene in SD-induced AF, indicating its promise as a biomarker and a target for therapy. Nonetheless, additional studies are required to investigate the direct link between the activation of YBX1 and NLRP3 inflammasomes. This research broadens our comprehension of SD's effects on AF and suggests new treatment approaches to reduce the heart-related dangers linked to lack of sleep.

## Data Sharing Statement

Datasets of this work are available from the corresponding authors as required.

## Ethics Approval Statement

All animal experiments were conducted following approval by the Animal Research Ethics Committee of the First Affiliated Hospital of Xinjiang Medical University (approval number: 230306-117). The procedures strictly adhered to the guidelines established by the National Institutes of Health for the Care and Use of Laboratory Animals, ensuring full compliance with ethical standards for animal research. Furthermore, the human samples utilized in this research adhered rigorously to the ethical standards set by the Medical Ethics Committee of Xinjiang Medical University's First Affiliated Hospital (Approval No. K202412-24) and adhered to the ethical principles outlined in the Declaration of Helsinki.

## Author Contributions

All authors made a significant contribution to the work reported, whether that is in the conception, study design, execution, acquisition of data, analysis and interpretation, or in all these areas; took part in drafting, revising or critically reviewing the article; gave final approval of the version to be published; have agreed on the journal to which the article has been submitted; and agree to be accountable for all aspects of the work.

## Funding

This work was supported by the National Natural Science Foundation [grant number 82370326, 82260065, 81873488], Xinjiang Uygur Autonomous Region Natural Science Foundation Project [grant number 2021D01E27,2022D01C767, 2022D01C578], "Youth Scientific Research Launch" Special Fund Project (2023YFY-QKMS-09), Xinjiang Uygur Autonomous Region Graduate Innovation Program [grant number XJ2024G147], Xinjiang Key Laboratory of Neurological Disorder Research [grant number XJDX1711-2253].

## Disclosure

The authors declare no conflicts of interest.

## References

1. Brundel BJM, Ai X, Hills MT, et al. Atrial fibrillation. *Nat Rev Dis Primers*. 2022;8(1):21. doi:10.1038/s41572-022-00347-9
2. Lau DH, Nattel S, Kalman JM, et al. Modifiable risk factors and atrial fibrillation. *Circulation*. 2017;136(6):583–596. doi:10.1161/CIRCULATIONAHA.116.023163
3. Ajuolabady A, Nattel S, Lip GYH, et al. Inflammasome signaling in atrial fibrillation: JACC state-of-the-art review. *J Am Coll Cardiol*. 2022;79(23):2349–2366. doi:10.1016/j.jacc.2022.03.379
4. Chen N, Guo L, Wang L, et al. Sleep fragmentation exacerbates myocardial ischemia–reperfusion injury by promoting copper overload in cardiomyocytes. *Nat Commun*. 2024;15(1):3834. doi:10.1038/s41467-024-48227-y
5. Huang T, Mariani S, Redline S. Sleep irregularity and risk of cardiovascular events: the multi-ethnic study of atherosclerosis. *J Am Coll Cardiol*. 2020;75(9):991–999. doi:10.1016/j.jacc.2019.12.054
6. Wong CX, Modrow MF, Sigona K, et al. Preceding night sleep quality and atrial fibrillation episodes in the I-STOP-AFIB randomized trial. *JACC Clin Electrophysiol*. 2023:S2405–500X(23)00729–6. doi:10.1016/j.jacep.2023.09.009
7. Tobaldini E, Costantino G, Solbiati M, et al. Sleep, sleep deprivation, autonomic nervous system and cardiovascular diseases. *Neurosci Biobehav Rev*. 2017;74(Pt B):321–329. doi:10.1016/j.neubiorev.2016.07.004
8. Simpson N, Dinges DF. Sleep and inflammation. *Nutr Rev*. 2007;65(12 Pt 2):S244–252. doi:10.1111/j.1753-4887.2007.tb00371.x
9. Liu H, Chen A. Roles of sleep deprivation in cardiovascular dysfunctions. *Life Sci*. 2019;219:231–237. doi:10.1016/j.lfs.2019.01.006
10. Sang D, Lin K, Yang Y, et al. Prolonged sleep deprivation induces a cytokine-storm-like syndrome in mammals. *Cell*. 2023;186(25):5500–5516.e21. doi:10.1016/j.cell.2023.10.025

11. Hu YF, Chen YJ, Lin YJ, et al. Inflammation and the pathogenesis of atrial fibrillation. *Nat Rev Cardiol.* 2015;12(4):230–243. doi:10.1038/nrcardio.2015.2
12. Churko JM, Mantalas GL, Snyder MP, et al. Overview of high throughput sequencing technologies to elucidate molecular pathways in cardiovascular diseases. *Circ Res.* 2013;112(12):1613–1623. doi:10.1161/CIRCRESAHA.113.300939
13. Peng C, Zhang Y, Lang X, et al. Role of mitochondrial metabolic disorder and immune infiltration in diabetic cardiomyopathy: new insights from bioinformatics analysis. *J Transl Med.* 2023;21(1):66. doi:10.1186/s12967-023-03928-8
14. Ritchie ME, Phipson B, Wu D, et al. Limma powers differential expression analyses for RNA-sequencing and microarray studies. *Nucleic Acids Res.* 2015;43(7):e47. doi:10.1093/nar/gkv007
15. Ito K, Murphy D. Application of ggplot2 to pharmacometric graphics. *CPT Pharmacometrics Syst Pharmacol.* 2013;2(10):e79. doi:10.1038/psp.2013.56
16. Kanehisa M, Goto S. KEGG: kyoto encyclopedia of genes and genomes. *Nucleic Acids Res.* 2000;28(1):27–30. doi:10.1093/nar/28.1.27
17. Kanehisa M, Furumichi M, Sato Y, et al. KEGG for taxonomy-based analysis of pathways and genomes. *Nucleic Acids Res.* 2023;51(D1):D587–D592. doi:10.1093/nar/gkac963
18. Kanehisa M. Toward understanding the origin and evolution of cellular organisms. *Protein Sci.* 2019;28(11):1947–1951. doi:10.1002/pro.3715
19. Yu G, Wang LG, Han Y, et al. clusterProfiler: an R package for comparing biological themes among gene clusters. *OMICS.* 2012;16(5):284–287. doi:10.1089/omi.2011.0118
20. Walter W, Sánchez-Cabo F, Ricote M. GPlot: an R package for visually combining expression data with functional analysis. *Bioinformatics.* 2015;31(17):2912–2914. doi:10.1093/bioinformatics/btv300
21. Langfelder P, Horvath S. WGCNA: an R package for weighted correlation network analysis. *BMC Bioinformatics.* 2008;9:559. doi:10.1186/1471-2105-9-559
22. Szklarczyk D, Gable AL, Nastou KC, et al. The STRING database in 2021: customizable protein-protein networks, and functional characterization of user-uploaded gene/measurement sets. *Nucleic Acids Res.* 2021;49(D1):D605–D612. doi:10.1093/nar/gkaa1074
23. Chin CH, Chen SH, Wu HH, et al. cytoHubba: identifying hub objects and sub-networks from complex interactome. *BMC Syst Biol.* 2014;8(Suppl 4):S11. doi:10.1186/1752-0509-8-S4-S11
24. Hao PY, Chiang JH, Chen YD. Possibilistic classification by support vector networks. *Neural Netw.* 2022;149:40–56. doi:10.1016/j.neunet.2022.02.007
25. Friedman J, Hastie T, Tibshirani R. Regularization paths for generalized linear models via coordinate descent. *J Stat Softw.* 2010;33(1):1–22. doi:10.18637/jss.v033.i01
26. Li Y, Yu J, Li R, et al. New insights into the role of mitochondrial metabolic dysregulation and immune infiltration in septic cardiomyopathy by integrated bioinformatics analysis and experimental validation. *Cell Mol Biol Lett.* 2024;29(1):21. doi:10.1186/s11658-024-00536-2
27. Nahm FS. Receiver operating characteristic curve: overview and practical use for clinicians. *Korean J Anesthesiol.* 2022;75(1):25–36. doi:10.4097/kja.21209
28. Newman AM, Liu CL, Green MR, et al. Robust enumeration of cell subsets from tissue expression profiles. *Nat Methods.* 2015;12(5):453–457. doi:10.1038/nmeth.3337
29. Zhu J, Chen C, Wu J, et al. Effects of propofol and sevoflurane on social and anxiety-related behaviours in sleep-deprived rats. *British Journal of Anaesthesia.* 2023;131(3):531–541. doi:10.1016/j.bja.2023.05.025
30. Sun H, Song J, Li K, et al. Increased  $\beta$ 1-adrenergic receptor antibody confers a vulnerable substrate for atrial fibrillation via mediating Ca<sup>2+</sup> mishandling and atrial fibrosis in active immunization rabbit models. *Clinical Science.* 2023;137(2):195–217. doi:10.1042/CS20220654
31. Sang W, Yan X, Wang L, et al. CALCOCO2 prevents AngII-induced atrial remodeling by regulating the interaction between mitophagy and mitochondrial stress. *International Immunopharmacology.* 2024;140:112841. doi:10.1016/j.intimp.2024.112841
32. Schroeder AB, Dobson ETA, Rueden CT, et al. The ImageJ ecosystem: open-source software for image visualization, processing, and analysis. *Protein Sci.* 2021;30(1):234–249. doi:10.1002/pro.3993
33. Elliott AD, Middeldorp ME, Van Gelder IC, et al. Epidemiology and modifiable risk factors for atrial fibrillation. *Nat Rev Cardiol.* 2023;20(6):404–417. doi:10.1038/s41569-022-00820-8
34. Liew SC, Aung T. Sleep deprivation and its association with diseases- a review. *Sleep Med.* 2021;77:192–204. doi:10.1016/j.sleep.2020.07.048
35. Lyabin DN, Eliseeva IA, Ovchinnikov LP. YB-1 protein: functions and regulation. *Wiley Interdiscip Rev RNA.* 2014;5(1):95–110. doi:10.1002/wrna.1200
36. Shah A, Lindquist JA, Rosendahl L, et al. Novel Insights into YB-1 signaling and cell death decisions. *Cancers (Basel).* 2021;13(13):3306. doi:10.3390/cancers13133306
37. Yu J, Wang W, Yang J, et al. LncRNA PSR regulates vascular remodeling through encoding a novel protein arteridin. *Circulation Research.* 2022;131(9):768–787. doi:10.1161/CIRCRESAHA.122.321080
38. Varma E, Burghaus J, Schwarzl T, et al. Translational control of Ybx1 expression regulates cardiac function in response to pressure overload in vivo. *Basic Res Cardiol.* 2023;118(1):25. doi:10.1007/s00395-023-00996-1
39. Xie Y, Wang Q, Yang Y, et al. Translational landscape of direct cardiac reprogramming reveals a role of Ybx1 in repressing cardiac fate acquisition. *Nat Cardiovasc Res.* 2023;2(11):1060–1077. doi:10.1038/s44161-023-00344-5
40. Zheng J, Liu P, Yang X. YB-1 immunization combined with regulatory T-cell depletion induces specific T-cell responses that protect against neuroblastoma in the early stage. *Acta Biochim Biophys Sin (Shanghai).* 2012;44(12):1006–1014. doi:10.1093/abbs/gms089
41. Zheng J, Jing W, Orentas RJ. Discovery of YB-1 as a new immunological target in neuroblastoma by vaccination in the context of regulatory T cell blockade. *Acta Biochim Biophys Sin (Shanghai).* 2009;41(12):980–990. doi:10.1093/abbs/gmp092
42. Kang S, Lee TA, Ra EA, et al. Differential control of interleukin-6 mRNA levels by cellular distribution of YB-1. *PLoS One.* 2014;9(11):e112754. doi:10.1371/journal.pone.0112754
43. Wicherska-Pawłowska K, Wróbel T, Rybka J. Toll-Like Receptors (TLRs), NOD-Like Receptors (NLRs), and RIG-I-Like Receptors (RLRs) in Innate Immunity. TLRs, NLRs, and RLRs Ligands as immunotherapeutic agents for hematopoietic diseases. *IJMS.* 2021;22(24):13397. doi:10.3390/ijms222413397
44. Hegdekar N, Sarkar C, Bustos S, et al. Inhibition of autophagy in microglia and macrophages exacerbates innate immune responses and worsens brain injury outcomes. *Autophagy.* 2023;19(7):2026–2044. doi:10.1080/15548627.2023.2167689

45. Chao YY, Puhach A, Frieser D, et al. Human TH17 cells engage gasdermin E pores to release IL-1 $\alpha$  on NLRP3 inflammasome activation. *Nat Immunol.* 2023;24(2):295–308. doi:10.1038/s41590-022-01386-w
46. Olsen MB, Gregersen I, Sandanger Ø, et al. Targeting the inflammasome in cardiovascular disease. *JACC Basic Transl Sci.* 2022;7(1):84–98. doi:10.1016/j.jacbts.2021.08.006
47. Zhang Y, Zhang S, Li B, et al. Gut microbiota dysbiosis promotes age-related atrial fibrillation by lipopolysaccharide and glucose-induced activation of NLRP3-inflammasome. *Cardiovasc Res.* 2022;118(3):785–797. doi:10.1093/cvr/cvab114
48. Heijman J, Muna AP, Veleva T, et al. Atrial myocyte NLRP3/CaMKII nexus forms a substrate for postoperative atrial fibrillation. *Circulation Research.* 2020;127(8):1036–1055. doi:10.1161/CIRCRESAHA.120.316710
49. Yao C, Veleva T, Scott L, et al. Enhanced cardiomyocyte NLRP3 inflammasome signaling promotes atrial fibrillation. *Circulation.* 2018;138(20):2227–2242. doi:10.1161/CIRCULATIONAHA.118.035202
50. Friebe J, Witkowski M, Wegner M, et al. Cytotoxic CD8+ T cells are involved in the thrombo-inflammatory response during first-diagnosed atrial fibrillation. *Cells.* 2022;12(1):141. doi:10.3390/cells12010141
51. Murakata Y, Yamagami F, Murakoshi N, et al. Electrical, structural, and autonomic atrial remodeling underlies atrial fibrillation in inflammatory atrial cardiomyopathy. *Front Cardiovasc Med.* 2022;9:1075358. doi:10.3389/fcvm.2022.1075358
52. Li X, Bao Y, Zhang N, et al. Senescent CD8+ T cells: a novel risk factor in atrial fibrillation. *Cardiovasc Res.* 2024;cvae222. doi:10.1093/cvr/cvae222
53. Hulsmans M, Schloss MJ, Lee IH, et al. Recruited macrophages elicit atrial fibrillation. *Science.* 2023;381(6654):231–239. doi:10.1126/science.abq3061
54. Momin N, Pabel S, Rudra A, et al. Therapeutic Spp1 silencing in TREM2+ cardiac macrophages suppresses atrial fibrillation. *Preprint. bioRxiv.* 2024:2024.08.10.607461. doi:10.1101/2024.08.10.607461
55. Ibarra-Coronado EG, Velázquez-Moctezuma J, Diaz D, et al. Sleep deprivation induces changes in immunity in *Trichinella spiralis* -infected rats. *Int J Biol Sci.* 2015;11(8):901–912. doi:10.7150/ijbs.11907
56. Wilder-Smith A, Mustafa FB, Earnest A, et al. Impact of partial sleep deprivation on immune markers. *Sleep Med.* 2013;14(10):1031–1034. doi:10.1016/j.sleep.2013.07.001
57. Massie A, Boland E, Kapás L, et al. Mice lacking alternatively activated (M2) macrophages show impairments in restorative sleep after sleep loss and in cold environment. *Sci Rep.* 2018;8(1):8625. doi:10.1038/s41598-018-26758-x
58. Ames C, Boland E, Szentirmai É. Effects of macrophage depletion on sleep in mice. *PLoS One.* 2016;11(7):e0159812. doi:10.1371/journal.pone.0159812

Journal of Inflammation Research

Publish your work in this journal

The Journal of Inflammation Research is an international, peer-reviewed open-access journal that welcomes laboratory and clinical findings on the molecular basis, cell biology and pharmacology of inflammation including original research, reviews, symposium reports, hypothesis formation and commentaries on: acute/chronic inflammation; mediators of inflammation; cellular processes; molecular mechanisms; pharmacology and novel anti-inflammatory drugs; clinical conditions involving inflammation. The manuscript management system is completely online and includes a very quick and fair peer-review system. Visit <http://www.dovepress.com/testimonials.php> to read real quotes from published authors.

Submit your manuscript here: <https://www.dovepress.com/journal-of-inflammation-research-journal>

**Dovepress**  
Taylor & Francis Group